Out-of-plane permeability measurement for reinforcement textiles: A benchmark exercise

A. X. H. Yong[a], A. Aktas[a], D. May[b], A. Endruweit[c], S. Advani[d], P. Hubert[e], S. G. Abaimov[f], D. Abliz[g], I. Akhatov[f], M. A. Ali[h], T. Allen[i], D.C. Berg[g], S. Bickerton[i], C. Brauner[j], D. Brütsch[j], B. Caglar[k], H. Caglar[l], P. Causse[m], A. Chiminelli[n], A. Cohades[k], S. Comas-Cardona[o], M. Danzi[p], J. Dittmann[q], C. Dransfeld[j], P. Ermanni[p], E. Fauster[r], J.A. Garcia- Manrique[s], A. George[t], R. Graupner[u], V. Grishaev[f], A. Guilloux[v], M. Hancioglu[l], W. Harizi[w], T. Herman[i], W. Huang[m], M.A. Kabachi[p], A. Keller[j], K. Kind[x], M. Laspalas[n], O. V. Lebedev[f], M. Lizaranzu[n], A.C. Long[c], K. Masania[j], V. Michaud[k], P. Middendorf[q], D. Salvatori[k], R. Schubnel[y], N. Sharp[z], M. Sozer[l], J. Thomas[h], F. Trochu[m], R. Umer[h], J. Valette[v], J. H. Wang[aa], B. Willenbacher[b]

[a] *National Physical Laboratory, UK*
[b] *Institut für Verbundwerkstoffe GmbH, Germany*
[c] *Composites Research Group, Faculty of Engineering, University of Nottingham, UK*
[d] *Department of Mechanical Engineering and Centre for Composite Materials, University of Delaware, USA*
[e] *Structures & Composite Materials Laboratory, McGill University, Canada*
[f] *Centre for Design, Manufacturing and Materials, Skolkovo Institute of Science and Technology, Russia*
[g] *Institute of Polymer Materials and Plastics Engineering, Technische Universität Clausthal, Germany*
[h] *Department of Aerospace Engineering, Khalifa University of Science and Technology, United Arab Emirates*
[i] *Centre for Advanced Composite Materials, University of Auckland, New Zealand*
[j] *Institute of Polymer Engineering, FHNW University of Applied Sciences and Arts Northwestern Switzerland, Switzerland*
[k] *Laboratory for Processing of Advanced Composites, Ecole Polytechnique Federale de Lausanne, Switzerland*
[l] *Composite Materials Manufacturing Laboratory, Mechanical Engineering Department, Koc University, Istanbul, Turkey*
[m] *Ecole Polytechnique Montreal, Canada*
[n] *Materials and Components Division, ITAINNOVA, Spain*
[o] *Research Institute in Civil Engineering and Mechanics (GeM), University of Nantes, France*
[p] *Laboratory of Composite Materials and Adaptive Structures, ETH Zürich, Switzerland*
[q] *Institute of Aircraft Design, University Stuttgart, Germany*
[r] *Processing of Composites Group, Montanuniversität Leoben, Austria*
[s] *Design for Manufacture Institute, Universitat Politecnica de Valencia, Spain*
[t] *Department of Manufacturing Engineering, Brigham Young University, USA*
[u] *Fraunhofer IGCV, Germany*
[v] *TENSYL, France*
[w] *Roberval (Mechanics, Energy and Electricity) Laboratory, Université de Technologie de Compiègne, France*
[x] *Chair of Carbon Composites (LCC), Technische Universität München, Germany*
[y] *Institut de Soudure Groupe, France*
[z] *Composite Manufacturing and Simulation Center (CMSC), Purdue University, USA*
[aa] *School of Materials Science and Engineering, Wuhan University of Technology, China*

Keywords: A. Fabric/textiles; B. Permeability; E. Liquid composite moulding; E. Resin flow

Abstract

The out-of-plane permeability of two glass fibre fabrics was measured by 26 institutions using silicone oil as a test fluid. Participants in this study were free to select the test procedure, specimen dimensions and data analysis method, provided that testing was carried out at three target fibre volume fractions, 46 %, 50 % and 54 %. While results showed a variability of two orders of magnitude between participants, most values were within a significantly narrower band. A majority of participants used 1D saturated test method. A few selected 1D unsaturated and 3D unsaturated flow method which gave very similar results. Focusing on analysis of data and results of 1D saturated flow measurements, results are not conclusive, but they are consistent with number of

layers in a specimen, fibre volume fraction, injection pressure and sealing of specimen edges all having an effect on the measured permeability. Specifying limits for these parameters is expected to result in reduced scatter in measured permeability.

1. Introduction

Liquid Composite Moulding (LCM) processes have seen an increase in popularity as manufacturers seek to exploit the benefits of reduced time, costs and energy over the more common prepreg/autoclave process at comparable product quality in terms of (high) fibre volume fraction and (low) void content. LCM encompasses a group of manufacturing techniques used to produce composite parts which all follow the principle of infusing a liquid polymer resin into a fibre reinforcement before curing, all within a mould which defines the finished part geometry. The flow of resin in LCM is frequently described by Darcy's law [1], which can be expressed as:

$$\mathbf{v} = -\frac{\mathbf{K}}{\mu}\nabla p \tag{1}$$

Here, $\mathbf{v}$ is a vector describing the phase-averaged flow velocity, $\mathbf{K}$ is a matrix describing the directional permeability of the reinforcement, μ is the dynamic viscosity of the (incompressible) resin, and ∇p is a flow-driving pressure gradient. The permeability depends on the geometrical arrangement of fibres in the reinforcement and on the fibre volume fraction, V_f. To assess process design to ensure complete saturation of the textile reinforcement during manufacture and to estimate cycle times, Eq. (1) can be used to predict the flow velocity. Frequently, numerical simulation techniques are employed to analyse resin flow, which require accurate data for the textile permeability as input. The permeability has different values in different material directions, in-plane and out-of-plane. As composites are frequently processed in thin shell-like structures, in-plane resin flow and the in-plane permeability of reinforcements have been extensively discussed. With increasing interest in the production of geometrically more complex thick structural parts applying LCM technology, and the development of processes such as SCRIMP (Seemann Composites Resin Infusion Molding Process) where the resin distributes across the reinforcement surface before impregnating the material through-thickness to minimize the flow distance [2], out-of-plane resin flow becomes more relevant.

The in-plane permeability is usually experimentally characterised independently of the out-of-plane permeability, and a standard test method will be developed following multiple international benchmarking trials for this type of measurement [3-5]. Out-of-plane permeability, K_z, also known as through-thickness permeability, is frequently characterised by measurement of the ratio between steady-state flow rate and pressure drop in flow of a chosen fluid through an already saturated fabric reinforcement, with the flow normal to the plane of the fabric structure,

i.e. in the thickness or the *z*-direction. Measurement of permeability in the out-of-plane direction can be more challenging than the in-plane due to the shorter distance of travel of the fluid and the impact of race tracking (in 1D tests). However, the main findings of the most recent in-plane permeability measurement benchmark exercise showed that cavity deformation was likely a significant contributor to variability in data between participants, as was the sensor location for pressure measurement. These principles can also be applied to measurement of the out-of-plane permeability. Transient flow (unsaturated, initially dry fabric) can be alternatively measured. It is worth noting that permeability measurement is not limited to separate in-plane and out-of-plane measurements, and a number of studies have been carried out to determine all components of permeability from a single experiment [6-8].

To date, no standard test method has been produced for measurement of the out-of-plane permeability. A survey carried out by the National Physical Laboratory and the National Composites Centre in the United Kingdom showed that standardisation of permeability measurement is considered long overdue by stakeholders from both industry and academia [9]. This work reports the results of an international benchmark exercise for out-of-plane permeability measurement, carried out in response to the need to begin the development of a standard test method. The 26 participants of this study are named in Table 1. The aim of this study was to determine the range of scatter in the measured K_z values and identify the cause of variability between the various permeability measurement techniques currently used. This will be the basis for providing guidelines for K_z measurement which will help develop a standard test method as it did for in-plane permeability testing.

2. Materials and Methods

2.1. Test procedures and set-ups

The participants of this study were free to use the experimental procedure and setup of their choice to carry out out-of-plane permeability measurements. Tests were carried out in either the saturated or unsaturated condition according to the preference of the participant. In total, 22 organisations carried out the test in the saturated state, and 6 in the unsaturated state (see Table 2). This includes two organisations, participants 9 and 22, who performed both types of test. A schematic diagram showing the principles of measurement in the 1D saturated, 1D unsaturated and 3D unsaturated methods of testing is given in Figure 1.

Participants carrying out the tests in the saturated condition typically used tools consisting of a stiff flow channel with a fluid inlet at one end and a fluid outlet at the other end, as described schematically by Wu et al. [10]. Specimens are compressed to a defined thickness by perforated plates, which allow parallel flow perpendicular to the fabric plane to develop such that the flow velocity is uniform on the channel cross-section. Pressure drop and

flow rate in the main direction of flow are measured. The out-of-plane permeability is then calculated using the following formulation of Darcy's Law in 1D:

$$Q = -\frac{K_z A}{\mu} \frac{\Delta p}{h} \tag{2}$$

Here, Q is the (volumetric) flow rate, A is the cross-sectional area of the flow channel, μ is the fluid viscosity, Δp is the difference in fluid pressure between both sides of the specimen, and h is the specimen thickness. For Eq. (2) to be applicable, it is important that a steady-state flow has been established, i.e. the specimen is fully saturated, and all air has been displaced from the flow channel. Fluid pressure and flow rate need to be monitored, and data for calculation of K_z can only be acquired once Δp and Q are constant. Potential issues with this type of set-up are:

- Gaps may form between the specimen and the flow channel walls resulting in artificially high flow rates [10]. To minimise this effect, typically known as race-tracking, it is generally recommended to apply a sealant to the edges of the specimens, e.g. silicone paste.
- The perforated plates may not be stiff enough and deform when the specimens are compressed, resulting in decreased fibre volume fraction.
- Specimens clamped between perforated plates may show local variations in thickness due to the uneven distribution of clamping pressure, which may affect the local fibre volume fraction and hence the permeability [11].
- The perforated plates may have a non-negligible influence on fluid flow resulting in increased pressure drop.

Aiming to avoid the effect of localised variations in specimen thickness due to the uneven distribution of clamping pressure (which may occur if perforated plates with a regular pattern of relatively large holes are used), participant 7 used a sintered porous medium instead of perforated plates for specimen clamping. It was confirmed experimentally that these plates did not cause a measurable pressure drop in a typical range of flow rates. Rather than attempting to seal gaps between specimen and tool walls, participant 7 used a flow channel geometry which separated flow at the edges of specimens from flow near the centre of specimens to eliminate the effect of race-tracking on the flow rate and on the calculated permeability [11]. Participants 8, 10 and 12 did not seal the specimen edges but applied localised specimen compression along the edges aiming at preventing race-tracking. Participants 1, 3, 11, 18 and 26 report use of a sealant at the specimen edges, while participant 16 use O-rings for sealing.

Participant 17 used a completely different method in saturated flow. Squeeze flow was induced by compressing previously saturated specimens between two platens. Pressure and compaction speed were determined instead of

fluid pressure and flow rate, which allowed K_z to be quantified at different V_f values in a single experiment [12]. However, the in-plane permeabilities, $K_x(V_f)$ and $K_y(V_f)$, need to be known for data analysis.

Six participants obtained K_z from tests carried out in the unsaturated condition and used a more diverse range of methods to calculate the permeability. Participants 9, 20 and 22 used set-ups similar to those typically used in saturated experiments. Based on tracking the flow front propagation between the perforated plates, the out-of-plane permeability was calculated using the 1D formulation of Darcy's law,

$$K_z = \frac{\varepsilon \mu z^2}{2\Delta p t} \ , \tag{3}$$

where z ($0 \le z \le h$) is the flow front position in thickness-direction, and t is the time for the flow front to reach position z. Notably, the porosity of the specimen, ε, where

$$\varepsilon = 1 - V_f \ , \tag{4}$$

needs to appear in the equations for calculation of unsaturated permeability, as this relates to the average flow velocity in the pore space. In calculation of the saturated permeability, this factor does not appear, as the phase-averaged velocity is used. Participants conducting unsaturated flow experiments generally tracked the flow front propagation visually. This can be challenging as the flow length is short (typically less than 10 mm) and accurate identification of the flow front position may not be straightforward. The tools used were (at least partially) made from transparent material. Participant 20 determined the time for the flow front to reach the specimen side opposite to the injection side (one data point for z and t). Participant 22 tracked the flow front propagation (continuously) from the side of the specimen. An exception in 1D flow is participant 9, who used electrical sensors to determine the time for the flow front to reach the side of the preform opposite to the injection side (one data point).

Participants 2, 13 and 21 used set-ups with a small-diameter injection gate on one side of the compacted specimen resulting in development of a semi-ellipsoidal flow front. They characterised the shape of 3D flow fronts and referenced equations given by Mekic et al. [13] or Becker et al. [14] for permeability calculation (Table 3). It is to be noted that the method for data reduction is significantly more complex than for the saturated 1D case described by Eq. (2), and that permeability results may differ based upon the choice of calculation method [5, 6, 13, 14]. For 3D flow experiments, the shape of the injection gate should ideally reproduce the ellipsoidal shape of the flow front (for short flow distances), which in practice is impossible. For long flow distances, the effect of the injection gate shape becomes less significant ("point injection"). However, if the specimen thickness is in the same order as the injection gate diameter, this does not apply. The method used by participant 21 also requires previous knowledge of the in-plane permeability values, K_x and K_y. Participants 2 and 21 determined the time for the flow front to reach the opposite side of the specimen visually (one data point). Participant 13 employed

ultrasound time-of-flight measurement to track the flow front propagation (continuously). However, due to signal loss, this method did not allow data to be acquired for all combinations of material and fibre volume fraction studied here. For all participants, it has been assumed that *z* is the principal flow direction during calculation of the permeability. While it would be possible to confirm this by means of a numerical study using detailed geometrical information on the fibre arrangement in the specimens, this additional study was not performed as it would have been outside of the scope of the present work, which centres on the reproducibility of experimental K_z measurements. Details of injection tools used, such as tool material, closing mechanism and cavity height control, varied between participants. These are listed in Tables 2 and 4 and summarised in Figure 2.

2.2. Materials

Two reinforcement fabrics were characterised in this benchmark exercise. The first was a biaxial ±45° E-glass fibre non-crimp fabric (with small amounts of fibres, 1 g/m^2 and 2 g/m^2, orientated in 0° and 90° directions, respectively) and a nominal areal weight of 444 g/m^2, supplied by Saertex. The second was a 2/2 twill woven E-glass fibre fabric with an areal weight of 295 g/m^2, supplied by Hexcel. The fabrics distributed between participants were taken from the same respective batch. Images of both fabrics are shown in Figure 3. Further details of these fabrics are described in the report for an international benchmarking exercise on the measurement of in-plane permeability [5].

The test fluid used in this trial was Dow Corning Xiameter PMX-200 100 cs silicone fluid. Silicone fluid was chosen as the model fluid as it offers a more stable viscosity than liquid resin. The viscosity of each batch of silicone fluid used in this study was measured as a function of temperature in a range from 15 °C to 40 °C (using an Anton Paar MCR 302 rheometer) by a single institution, TU Munich. The fluid temperature was measured by each participant prior to or during testing, and the viscosity was derived from the viscosity-temperature curve. This test fluid was used by all participants with the exception of participants 9 and 11 who used different model fluids. Participant 9 used a soluble polymer in water, as the sensors used in their test setup required a conductive fluid and therefore the recommended silicone oil was not suitable. Participant 11 used Shell Telius 46 hydraulic oil. Participant 18 reported that an ultrasound flow meter could not be used for measuring the flow rate of the silicone fluid. This was attributed to the velocity of sound in this specific fluid.

2.3. Specimen preparation

Three target fibre volume fractions, 46 %, 50 % and 54 %, were specified for this trial. All participants were asked to carry out a minimum of five repeats at each V_f. They were free to select the number of fabric layers in the

specimens, n, and the cavity height in the measurement tool, h, used to achieve these V_f values. They were instructed to ensure that the fibre directions in all layers were aligned and that the orientation of the fabric was the same in all layers. Specimen dimensions were not set. The details of the specimen dimensions for each participant and the combination of n and h to determine V_f according to

$$V_f = \frac{A_w n}{h\rho} \quad , \tag{5}$$

where A_w is the areal density of the reinforcement fabric, and ρ is the density of the fibre material, are given in Table 5. Here, the value for ρ was given as 2550 kg/m^3 (for E-glass).

Reported sample thicknesses ranged from 1.1 mm to 14.6 mm across the participants. Numbers of fabric layers in the specimens were between 5 and 50 (Figure 4). The sample geometries also varied, with 20 participants using round specimens, 5 using square specimens and one participant using elliptical specimens. Each specimen was weighed prior to testing. The fibre volume fractions in the tool were calculated using the equation

$$V_f = \frac{m}{Ah\rho} \quad , \tag{6}$$

where m is the specimen mass. It is to be noted that values of V_f calculated using Eqs. (5) and (6) were not always identical. However, differences were typically small (≤ 2 %).

A general problem when cutting fabric specimens is that the material may fray along the specimen edges, and individual fibre bundles may be lost. Particularly for the woven fabric, the low shear resistance of the material may have caused issues when specimens were handled. This can result in a reduction of the effective specimen dimensions and of the effective specimen mass. Both effects need to be considered when the tests are carried out. It was also reported (participants 14 and 18) that the woven fabric deformed when trying to squeeze a large number of layers into the flow channel, which made experiments impossible or may have affected the reliability of K_z at high V_f.

Most participants used a new specimen for each test. Participant 24 used the same specimen at increasing levels of compaction for measurement of permeability at all three target fibre volume fractions. Participant 17 produced continuous results for K_z as a function of V_f for each tested specimen.

2.4 Test parameters

For the out-of-plane permeability tests, a set injection pressure was used by 23 participants, while 2 participants (participants 18 and 24) used a set flow rate. The pressure was typically set using pressure pots, while the flow rate was set using pumps. The fluid was injected from below the specimens by 22 participants. Participant 2

injected from above, and participant 4 injected the fluid with the fabric *z*-direction oriented horizontally. Participant 17 did not carry out the measurements via a fluid injection and instead pressed the fluid through the thickness of the fabric stack using compression. The details of each participant setup are given in Table 2.

In saturated flow experiments, steady-state flow develops, where both injection pressure and flow rate are constant. Hence, it is not relevant which one is set. As indicated in Eq. (2), pressure difference and flow rate are used to calculate K_z based on saturated flow experiments. As it is not clear how the target values of pressure or flow rate, set using a pressure pot or pump, correspond to the true values in the permeability measurement tool, monitoring the true values is necessary during a test. Participant 24 set the flow rate, but did not monitor the true values, which may have affected the accuracy of the measurement. The pressure difference is typically measured using pressure readings from inside the tool. 14 participants measured the pressure on both sides of the tool, 7 on the inlet side only. Depending on the design of the tool, pressure may not only build up at the inlet side ("upstream" of the specimen), but also at the outlet ("downstream"). Hence, the accuracy of the measured pressure difference is expected to be higher when fluid pressure is measured on both sides of the specimen. The flow rate is measured either directly, using a flow meter (3 participants), or indirectly, measuring the change in mass of test fluid passing through the set-up (16 participants). For indirect flow rate measurement, the mass of the pressure pot (2 participants) or of a collection pot at the tool outlet (14 participants) was monitored as a function of time. The flow rate was then calculated from the slope of a line fitted to the data.

In unsaturated flow experiments, where K_z is calculated according to Eq. (3) or the equations listed in Table 3, the pressure difference is typically given, and the flow rate is determined by flow front tracking. In practice, Δp is determined by measuring the fluid pressure at the injection gate and subtracting the atmospheric pressure on the flow front. Typically, only the injection pressure is measured. As the flow front propagation is tracked, the flow rate, which decreases with time, does not need to be monitored (participant 13 employed flow front tracking and flow rate monitoring).

Flow-driving fluid pressure differences between both sides of the specimen were typically in the order of 100 kPa. The highest reported values of Δp were approximately 450 kPa (participant 9). Participant 26 used gravity-driven fluid injection at a value of Δp of 5 kPa.

3. Results

3.1. Summary of recorded data

The results of the permeability measurements are presented in Figure 5. For each participant and each fibre volume fraction, average permeability values are in the range between 8.3×10^{-14} m^2 and 7.5×10^{-12} m^2 at 45 % ≤ V_f ≤ 47 %, 5.4×10^{-14} m^2 and 5.4×10^{-12} m^2 at 49 % ≤ V_f ≤ 51 %, and 1.2×10^{-13} m^2 and 4.6×10^{-12} m^2 at 53 % ≤ V_f ≤ 55 % for the woven fabric. For the NCF, values were between 2.7×10^{-13} m^2 and 7.4×10^{-12} m^2 at 45 % ≤ V_f ≤ 47 %, 1.4×10^{-13} m^2 and 8.6×10^{-12} m^2 at 49 % ≤ V_f ≤ 51 %, and 2.4×10^{-13} m^2 and 4.6×10^{-12} m^2 at 53 % ≤ V_f ≤ 55 %. The standard deviations for each individual data series are between 6×10^{-15} m^2 and 4×10^{-12} m^2 (woven fabric) and between 5×10^{-15} m^2 and 6×10^{-12} m^2 (NCF). Broadly, the standard deviation of K_z in each individual test series tends to decrease with increasing V_f. This may be related to higher numbers of layers being used at higher V_f, which minimises the scatter related to variable nesting between layers. While the data indicate a scatter of up to two orders of magnitude (similar to a previous benchmark study, where test parameters were not prescribed [3]), most results in Figure 5 are in fact clustered in a much narrower band where the ratio between upper bound and lower bound at any fibre volume fraction is approximately 4.

While three target fibre volume fractions were specified in this exercise, 46 %, 50 % and 54 % (Section 2.3), data returned by participants show four distinct clusters representing V_f values in the ranges of 43 % to 47 %, 48 % to 51 %, 52 % to 56 % and > 56 %. A major source of difference between the fibre volume fractions achieved by participants was the combination of number of layers and respective cavity height used. As seen in Table 5, some participants used different number of layers at the same cavity height, and vice versa, for example participants 1 and 4, who both used 12, 13 and 14 layers of fabric to achieve the three V_f values, but with different cavity heights of 2.91 mm and 3 mm, respectively.

3.2. Kozeny-Carman fit

For easy comparison of data, a fit was applied to measured data using the average K_z obtained at every V_f by each participant. For the fit, the Kozeny-Carman equation [15], which is sometimes used to approximate the dependence of the permeability of reinforcements on the fibre volume fraction, was used as follows:

$$K_z = k_0 \frac{(1-V_f)^3}{V_f^2} \quad . \tag{7}$$

While this equation was originally derived for the permeability of porous media consisting of spherical particles, not for the permeability of (structured) fibrous media, it describes the most important characteristics, a decrease in permeability with increasing V_f where the slope of the $K_z(V_f)$ curve flattens continuously. The measured permeability values were plotted against the values for $(1\text{-}V_f)^3/V_f^2$, which were calculated for each participant using the measured V_f data. Next, a linear regression was applied to obtain the coefficient, k_0 (Figure 6). The

quality of each fit was checked using the coefficient of correlation, R^2. Values for k_0 and R^2 are listed in Table 6 and plotted in Figure 7. Here, the Thompson Tau test was employed to identify potential outliers.

The values for k_0 allow easy comparison of the data obtained by different participants quantitatively (based on only one parameter), while R^2 indicates how well the experimental data follow the theoretical approximation. Values of R^2 near 1 indicate that data follow the expected continuous decrease in K_z with increasing V_f. For data series where R^2 is significantly smaller than 1, individual data points do not lie on the fit curve (i.e. they may not follow the expected trend), which could be an indication for issues with the experiments. While applicability of Eq. (7) cannot be taken for granted, results in Table 6 show that it fits the experimental data well, i.e. values of R^2 are near 1, for most data series. This indicates that the dependence of K_z on V_f expressed in the Kozeny-Carman equation generally describes the trends observed for the fabrics characterised here. If the potential outliers are ignored, values for k_0 are in the range between 0.17×10^{-12} m^2 and 2.86×10^{-12} m^2 for the woven fabric and between 2.65×10^{-12} m^2 and 9.34×10^{-12} m^2 for the NCF. It is to be noted that it may still be possible to find a good fit to a data set (i.e. high values of R^2), even if it contains outliers.

3.3. Fit with analytical equations

In addition, to check the applicability of simple analytical models for transverse flow through an array of cylinders, the value of K_z obtained at V_f = 46 %, 50 % and 54 %, for an average glass fibre radius of r = (4.13±0.47) µm, measured on a high-resolution X-ray tomographic image of a bundle extracted from the Hexcel fabric, was calculated using the model of Gebart for flow through a quadratic or an hexagonal array [16]. The results range from $(0.40\pm0.09)\times10^{-12}$ m^2 for 46 % to $(0.11\pm0.02)\times10^{-12}$ m^2 for 54 % for the square array and $(0.45\pm0.10)\times10^{-12}$ m^2 for 46 % to $(0.17\pm0.04)\times10^{-12}$ m^2 for 54 % for the hexagonal array, which is roughly in the right order of magnitude but, as expected, lower than the experimentally measured values as this model does not take into account the dual-scale nature of the fabrics. More advanced analytical models would bring closer estimates, however they are not the focus of the present benchmark. Whilst an exact analytical solution for the permeability of the fabrics studied here cannot be found, detailed geometrical models of the reinforcement architecture could be generated based on micro-CT data which could then be used as input for numerical flow simulations. These could be used to derive the permeability for the fibre structure.

4. Discussion

4.1 Effect of test method

To identify the effect of different experimental parameters, all data (Figure 5) were divided into groups of participants, according to the parameters they used in their tests. For the acquired data for $K_z(V_f)$, the full range of

V_f was divided into several intervals. For each interval, average values and standard deviations for K_z and V_f were calculated for the identified groups of participants (based on average values reported by each participant). Data series based on results from a single participant are indicated using the averages and standard deviations reported for these results.

Figure 8 shows a comparison of data for the different experimental approaches used. The figure shows that data acquired in 1D saturated, 1D unsaturated and 3D unsaturated flow tend to lie in the same ranges at all V_f. Only at $V_f \approx 0.47$ are the values obtained in 3D unsaturated tests higher. This is related to increased uncertainty, as only two participants (2 and 21) conducted tests in 3D unsaturated flow at this V_f (as mentioned above, participant 13 could not acquire data at all V_f). Compared to data obtained using other methods, K_z obtained by participant 17 in compression flow shows higher values for the woven fabric and lower values for the NCF (note: as only one participant used this method, averages and standard deviations refer to the series of tests at each V_f). The fact that the compression flow method is fundamentally different from the other methods, which use constant cavity height and V_f, may explain why these values are different. Figure 7 also indicates that values for k_0 lie in the same range for the majority of participants (ignoring outliers) using 1D saturated and 1D unsaturated flow experiments. Values of k_0 for 3D unsaturated flow experiments are also in the same range, but the value for compression flow is significantly higher for the woven fabric and near the lower end of the range for the NCF. For data obtained using 3D unsaturated flow experiments, values for R^2 tend to be smaller than for other experimental methods, suggesting less consistency in data for this method.

Participants 9 and 22 conducted experiments in both 1D saturated and 1D unsaturated flow. Figure 9 shows that agreement between values from both methods is very good for participant 9 (this participant measured unsaturated and saturated permeability in one continuous experiment). For participant 22, there is a larger difference between data from both methods. Values obtained in 1D saturated tests tend to be larger than those from 1D unsaturated tests for woven fabric, but it tends to be the other way around for the NCF. Hence, these data show no clear difference between both methods. It is also to be considered that both participants used different test fluids (participant 9: water-based solution; participant 22: silicone fluid), which may lead to different capillary forces acting during unsaturated measurements.

In summary, permeability tests in 1D saturated flow, 1D unsaturated flow and 3D unsaturated flow appear to give very similar results, while results from compression flow tests are significantly different. An implication is that K_z values obtained in 1D saturated flow experiments can be used to approximate unsaturated flow in LCM

processing. In the following discussion, detailed evaluation of data will focus on the 1D saturated flow method, as this was used by the largest number of participants.

4.2 Effect of injection pressure

Here, average values and standard deviations were calculated for a group of seven participants who conducted the tests consistently at pressure differences near Δp = 100 kPa. Data related to outliers in k_0 were not included here. The values for this group were compared with results for participant 26, who conducted the tests at much lower pressures (Δp = 5 kPa), and for participant 22, who used higher pressures, up to Δp = 450 kPa. Figure 10 shows that participant 26 obtained significantly smaller permeability values ($k_0 = 0.17\times10^{-12}$ m^2 for woven fabric, $k_0 = 0.30\times10^{-12}$ m^2 for NCF) than those obtained at Δp = 100 kPa (average $k_0 = 1.85\times10^{-12}$ m^2 for woven fabric, average $k_0 = 4.90\times10^{-12}$ m^2 for NCF). As pressure difference and flow rate were very low in the experiments conducted by participant 26, it is possible that limited accuracy of measurement equipment (pressure sensors and scales for measurement of mass flow) may have affected the results. However, one of the participants using a pressure difference of approximately 100 kPa also obtained values of $K_z(V_f)$ and of k_0 similar to those obtained by participant 26 (as may be seen in Figure 5), which suggests that low measurement accuracy related to the small Δp may not be the only cause of deviating permeabilities here. Permeability values reported for high injection pressure (participant 22) are similar to those at Δp = 100 kPa for the woven fabric ($k_0 = 1.19\times10^{-12}$ m^2). For the NCF, results for participant 22 ($k_0 = 7.15\times10^{-12}$ m^2) at V_f = 0.47 are very similar to the values measured at Δp = 100 kPa, but the decrease in K_z at higher V_f is significantly smaller than at the lower pressure. The small value of R^2 (Table 6) suggests that the accuracy for this data series may be affected by variables other than Δp, but the source of deviation is not obvious.

A general issue with all configurations for through-thickness injection experiments is that the applied fluid pressure may deform the specimen locally and change the fibre volume fraction [10, 17]. As this may affect the permeability, the fluid pressure should not exceed the specimen compaction pressure. On the other hand, pressure and flow rate need to be high enough to allow accurate readings to be obtained with the available measurement equipment (see above).

Rough estimates based on results from a recent compressibility study [18] suggest that values of the compaction pressure to obtain fibre volume fractions of 46 %, 50 % and 54 % are in the order of 50 kPa, 100 kPa and 200 kPa for the NCF and in the order of 25 kPa, 50 kPa and 100 kPa for the woven fabric. Using an injection tool which allows monitoring the true specimen thickness [19], participant 10 observed average reductions in true specimen

thickness of 0.04 mm, 0.01 mm and 0.01 mm for the NCF (at target thicknesses of 3.80 mm) at a fluid pressure difference of 100 kPa and at target fibre volume fractions of 46 %, 50 % and 54 %, respectively. For the woven fabric, average thickness reductions were 0.06 mm, 0.02 mm and 0.01 mm (at target thicknesses of 3.70 mm, 3.50 mm and 3.60 mm), respectively. This is consistent with a reduction in specimen thickness if Δp is greater than the specimen compaction pressure. The absolute value of the thickness reduction increases with increasing difference between Δp and compaction pressure. If Δp is smaller than the specimen compaction pressure, no significant reduction (0.01 mm) in specimen thickness is observed. For participant 10, the thickness reductions correspond to maximum increases in fibre volume fraction by approximately 1 %. In cases where higher values of Δp were used, more significant effects of preform compaction may have occurred.

Two participants used several combinations of pressure and flow rate for each specimen, but the submitted data do not allow to draw any conclusion with respect to the effect of the pressure on the measured permeability. Participant 18 injected the fluid at set flow rate, while other participants set the injection pressure. As expected, the results do not differ from those obtained at set pressure (tests are run in steady-state flow).

4.3 Effect of cavity height control method

The cavity height for each 1D test rig was set through either displacement of a universal test machine (UTM), which provided dynamic cavity height control, or static methods using spacers of given thickness or bolts. The only exception was the test rig used by participant 9, which had a fixed cavity height. Use of a UTM to set and hold the cavity height also enables monitoring of changes in cavity height under the injection pressure, sometimes with the help of Linear Variable Differential Transformers (LVDTs). In Figure 11, the methods for setting the cavity height are compared. The results show that no distinct relationship between the method used to set (and/or monitor) the cavity height and the measured K_z for each V_f interval can be identified (i.e. the scatter along the k_0-axis is similar in Figure 11), and it is therefore not possible to identify a clear advantage for either control method with respect to accuracy of K_z measurement.

4.4 Effect of specimen geometry

Specimens were either circular or square, with the exception of participant 10 who used elliptical specimens. Figure 12 shows a comparison of values of k_0, with participants grouped by geometry (circle, square or ellipse). No clear influence from the shape of the specimen can be identified in these data. In addition to variations in specimen shape, the in-plane area of the specimens was spread across a wide range, from 100 mm^2 to 49087 mm^2 for participants who carried out 1D saturated tests. This was related to values of k_0 in Figure 13. As with the

specimen shape, there was no identifiable relationship between the in-plane area of the specimens and K_z measured by participants. As the theory does not suggest that there should be any effect of specimen shape or size on permeability, the observations suggest that there were no significant secondary effects which could have affected the true permeability.

4.5 Effect of edge sealing

Tests carried out in 1D flow can be susceptible to race-tracking, i.e. flow around the edge of the specimen rather than through the thickness. Out of the participants where detailed information was available, participants 1, 3, 11, 16, 18 and 26 applied a sealant tape, silicone layer or O-ring to seal the edge of each specimen to mitigate race-tracking. It is to be noted that applying sealant does not guarantee that race-tracking is completely prevented and relies on the skill of the user for neat application. Participants 8, 10 and 12 applied localised compression, and participant 7 employed a strategy of flow separation to minimise the effect of edge flow on the measured K_z (see Section 2.1). The remainder of the participants did not report any details of methods used to restrict flow at the edges other than cutting the specimens with a good fit to the inner flow channel diameter. Figure 14 shows a comparison of k_0 for participants who employed mitigation strategies (i.e. edge sealing, compression or flow separation) with participants known not to have applied any method for physical restriction of flow at the specimen edge. These data show that, for the woven fabric, the scatter in k_0 is similar for specimens with edge sealing or clamping as for participants who did not attempt to minimise effects of edge flow (if outliers are ignored). For the NCF, the scatter is also similar, but values of R^2 tend to be smaller for specimens with no sealing than for specimens with sealing or edge clamping. Permeabilities resulting from the flow separation method are similar to those from edge sealing for the woven fabrics, but higher for the NCF.

4.6 Effect of distribution medium

In 1D flow experiments for measurement of K_z, reinforcement specimens are compressed to a defined thickness between two plates, which also need to facilitate (parallel) fluid flow through the specimens. Results for participants using different compaction plates/distribution media are compared in Figure 15, for those participants where detailed information on the plates was given. Data related to outliers in k_0 were not included here. Three participants were identified as using plates with small holes (2 mm to 3 mm diameter), three participants used plates with larger holes (6 mm to 8 mm diameter), participant 7 used a sintered porous medium, and participant 15 used plates with large holes of unspecified size. It is to be noted that average values and standard deviations were calculated for the purpose of visualisation of results, although, strictly speaking, this is questionable for

series of only three data points. Particularly for the woven fabric, permeability data show large scatter (Figure 15a). However, results obtained using different compaction plates/distribution media are generally similar, particularly at fibre volume fractions greater than 0.50. No clear trend can be identified for results obtained using different compaction plates. Similarly, values for k_0 do not show any clear trend.

4.7 Effect of specimen stack height

Participants used a wide range of stack heights to achieve the target V_f values, as was shown in Figure 4 and Table 5. One of the considerations for the selection of the stack height for testing includes limitations in the cavity height of the test rig. Many participants maintained a fixed cavity height whilst altering the number of layers of fabric to obtain the target V_f. In addition to physical limitations of the test rig, it is possible that at a low number of fabric layers, local changes in thickness that occur at the fluid inlet locations would create a more significant influence in the measurement outcome. At higher numbers of layers, laying up and aligning multiple layers in a fabric stack and placement within the test rig become more challenging. On the other hand, different configurations of nesting between layers would be expected to cause larger scatter in results for low numbers of layers, while convergence, i.e. smaller scatter, would be expected at high numbers of layers. In Figure 16, the data are grouped by the number of layers used by participants in each fabric stack. Here, the values for k_0 and R^2 are plotted to best assess the impact of the fabric stack height on the data. The data indicate that there is a greater number of outliers for low numbers (5 to 15 layers and 15 to 25 layers) than for larger numbers (with the exception of one outlier, which also has a low R^2) for the woven fabric. This observation is consistent with a significant effect of nesting between layers causing larger scatter at low numbers, while convergence is achieved for higher numbers of layers. For the NCF, there appears to be no clear effect of the number of layers on the scatter in results. This is consistent with no nesting occurring between fabric layers. As fibre bundles orientated at 45° (in one layer) are in contact with fibre bundles at -45° (in another layer), i.e. fibre bundles from different layers are orientated at 90° relative to each other, no nesting can occur between layers.

4.8 Impact of variables

A single-factor analysis of variance (ANOVA) test was carried out on the k_0 data for the 1D saturated tests (with and without outliers identified through the Thompson Tau test) for the effect of pressure monitoring method, sensor location, flow rate monitoring method, edge sealing and number of layers. The ANOVA test is a statistical analysis method that enables the user to assess the impact of chosen variables on mean values [20]. In all cases,

the results showed that there was no significant effect of the factors on the results. Evaluation of the data is not conclusive due to the high number of confounding factors.

5. Conclusions

A diverse range of approaches was used to measure the out-of-plane permeability of two glass fibre fabrics at three target fibre volume fractions. In the reported experimental data for the through-thickness permeability, a large scatter (two orders of magnitude) is observed between data obtained by different participants, similar as observed in the first benchmarking exercise for in-plane permeability measurement. However, most results lie in a much narrower band where the factor between minimum and maximum values of K_z at any fibre volume fraction is approximately 4. This band becomes even narrower at higher fibre volume fractions.

A Kozeny-Carman fit was applied to experimental data to enable an easy comparison in order to identify any variables which acted as a source of the variation. The fit was found to describe the dependence of K_z on V_f generally with good accuracy. A comparison of the methods used to measure K_z (1D saturated, 1D unsaturated, 3D unsaturated and compression flow) showed that for tests carried out in 1D and 3D there was no significant difference in the average result, while the values obtained in compression flow differed from those obtained through injection-based methods.

Focusing on measurement of K_z in 1D saturated flow, which was used by the majority of participants, available information on test parameters did not allow to identify clearly which parameters have a strong influence on the results. This was supported by a single-factor ANOVA test which showed that there was no significant effect of pressure monitoring method, sensor location, flow rate monitoring method, edge sealing and number of layers on the results due to the high number of confounding factors. Although this evaluation of the data is not conclusive, the following recommendations can be made based on fundamental theoretical considerations which are consistent with the reported observations:

- Sealing of specimen edges or other methods need to be employed to minimise race-tracking. Otherwise, this will result in artificially high flow rates and hence in inaccurate K_z values.
- Depending on the architecture of the reinforcement, nesting may occur at the interfaces between layers. As different nesting configurations can result in scatter in the K_z values, the number of layers used in the tests should be high to reduce the influence of nesting on the value measured.
- The flow rate, which affects the derived K_z value, needs to be in a range where it can be measured accurately. Hence, the injection pressure needs to be sufficiently high. On the other hand, the pressure must be lower

than the material-specific pressure required to further compact the specimen, which would result in an increase in V_f and a reduction in K_z. A pressure in the range of 100 to 200 kPa would be recommended.

- To assess the plausibility of data, geometrical unit-cell models can be used to numerically calculate K_z for comparison with the experimental results.

Specimen shape and size, the mechanism for setting the cavity height, and the type of the compression plates are not expected to affect the permeability measurement, and no effect was observed.

In addition to these theoretical considerations, processing and comparison of test reports and data from each participant showed that documentation of test setup and evaluation of test data during calculation of K_z is crucial for traceability of data and to increase the reproducibility of out-of-plane permeability measurements. In the absence of standardisation, this study provided an overview of test methods and data reduction schemes used for through-thickness permeability measurement. Aiming at formulating a test standard, an experimental design in which the variables are more controlled will be required in future work to better analyse sources of variations and improve reproducibility of results.

Acknowledgements
The authors thank Hexcel Corporation and Saertex GmbH for supplying the materials used in this exercise free of charge. The authors would also like to thank Santiago Miguel (Itainnova), Brad Buttars and Collin Childs (Brigham Young University) and Maik Theisig (University of Auckland) for specimen preparation and their contribution towards the experimental work, Louise Wright (NPL) for her assistance in data analysis, and Argyro Martidi (NPL) for her contribution to the data processing.

References

[1] Darcy H. Les Fontaines Publiques de la Ville de Dijon. Paris: Victor Dalmont; 1856.
[2] Han K, Jiang S, Zhang C, Wang B. Flow modeling and simulation of SCRIMP for composites manufacturing. *Compos Part A-Appl S*, 2000; 31(1): 79-86.
[3] Arbter R, Beraud JM, Binetruy C, Bizet L, Bréard J, Comas-Cardona S, Demaria C, Endruweit A, Ermanni P, Gommer F, Hasanovic S, Henrat P, Klunker F, Laine B, Lavanchy S, Lomov SV, Long A, Michaud V, Morren G, Ruiz E, Sol H, Trochu F, Verleye B, Wietgrefe M, Wu W, Ziegmann G.. Experimental determination of the permeability of textiles: a benchmark exercise. *Compos Part A-Appl S*, 2011, 42(9):1157-1168.
[4] Vernet N, Ruiz E, Advani S, Alms JB, Aubert M, Barbuski M, Baran B, Beraud JM, Berg DC, Correia N, Danzi M, Delavière T, Dickert M, Di Fratta C, Endruweit A, Ermanni P, Francucci G, Garcia JA, George A, Hahn C, Klunker F, Lomov SV, Long A, Louis B, Maldonado J, Meier R, Michaud V, Perrin H, Pillai K, Rodriguez E, Trochu F, Verheyden S, Wietgrefe M, Xiong W, Zaremba S, Ziegman G.. Experimental determination of the permeability of engineering textiles: Benchmark II. *Compos Part A-Appl S*, 2014, 61:172-184.
[5] May D, Aktas A, Advani SG, Endruweit A, Fauster E, Lomov SV, Long A, Mitschang P, Abaimov S, Abliz D, Akhatov I, Allen TD, Berg DC, Bickerton S, Bodaghi M, Caglar B, Caglar H, Correia N, Danzi M, Dittmann J, Ermanni P, George A, Grishaev V, Kabachi MA, Kind K, Lagardère MD, Laspalas M, Liotier PJ, Park CH, Pipes RB, Pucci M, Raynal J, Rodriguez ES, Schledjewski R, Schubnel R, Sharp N, Sims G, Sozer EM, Umer R, Willenbacher B, Yong A, Zaremba S, Ziegmann G. In-plane permeability characterization of engineering textiles based on radial flow experiments: a benchmark exercise. *Compos Part A-Appl S*, 2019, 121:100-114.
[6] Ahn SH, Lee WI, Springer GS. Measurement of the Three-Dimensional Permeability of Fiber Preforms Using Embedded Fiber Optic Sensors. *J Compos Mater*, 1995; 29(6): 714-733.

[7] Nedanov PB, Advani SG. A method to determine 3D permeability of fibrous reinforcements. *J Compos Mater*, 2002; 36(2): 241-254.
[8] Yun M, Sas H, Simacek P, Advani SG. Characterization of 3D fabric permeability with skew terms. *Compos Part A-Appl S*, 2017; 97: 51–59.
[9] Aktas A, Sims G, Lira C, Stojkovic M. NPL REPORT MAT 82: Survey of procedures in use for permeability measurements in liquid composite moulding processes. Teddington: National Physical Laboratory, 2016.
[10] Wu CH, Wang TJ, Lee LJ. Trans-Plane Fluid Permeability Measurement and Its Applications in Liquid Composite Molding, *Polym Composite*, 1994; 15(4): 289-298.
[11] Graupner R, Drechsler K. Quantitative transversal permeability testing - challenges and enhancements. In: The 14th International Conference on Flow Processing in Composite Materials, Lulea, 2018.
[12] Comas-Cardona S, Binetruy C, Krawczak P. Unidirectional compression of fibre reinforcements. Part 2: A continuous permeability tensor measurement. *Compos Sci Technol*, 2007; 67(3–4): 638-645.
[13] Mekic S, Akhatov I, Ulven C. A radial infusion model for transverse permeability measurements of fiber reinforcement in composite materials. *Polym Composite*, 2009; 30: 907-917.
[14] Becker D, Grössing H, Konstantopoulos S, Fauster E, Mitschang P, Schledjewski R. An evaluation of the reproducibility of ultrasonic sensor-based out-of-plane permeability measurements: a benchmarking study. *Advanced Manufacturing: Polymer & Composites Science*, 2016; 2(1): 34-45.
[15] Carman PC. Fluid flow through granular beds. *T I Chem Eng-Lond*, 1937; 15: 150-156.
[16] Gebart, B.R., Permeability of unidirectional reinforcement for RTM. *Journal of composite materials*, 1992; 26(8): 1100-1133.
[17] Trevino L, Rupel K, Young WB, Liou MJ, Lee LJ. Analysis of Resin Injection Molding in Molds With Preplaced Fiber Mats. I: Permeability and Compressibility Measurements. *Polym Composite*, 1991; 12(1): 20-29.
[18] Yong AXH, Aktas A, May D, Endruweit A, Lomov SV, Advani S, Hubert P, Abaimov SG, Abliz D, Akhatov I, Ali MA, Allaoui S, Allen T, Berg DC, Bickerton S, Caglar B, Causse P, Chiminelli A, Comas-Cardona S, Danzi M, Dittmann J, Dransfeld C, Ermanni P, Fauster E, George A, Gillibert J, Govignon Q, Graupner R, Grishaev V, Guilloux A, Kabachi MA, Keller A, Kind K, Large D, Laspalas M, Lebedev OV, Lizaranzu M, Long AC, López C, Masania K, Michaud V, Middendorf P, Mitschang P, van Oosterom S, Schubnel R, Sharp N, Sousa P, Trochu F, Umer R, Wanga JH. Experimental characterisation of textile compaction response: a benchmark exercise. *Compos Part A-Appl S*, 2021; 142: 106243.
[19] Becker D, Mitschang P. Measurement system for on-line compaction monitoring of textile reaction to out-of-plane impregnation. *Adv Compos Lett*, 2014; 23(2): 32-36.
[20] Box GEP, Hunter WG, Hunter JS Statistics for Experimenters: Design, Innovation, and Discovery, 2nd ed. New York, Wiley, 2005.

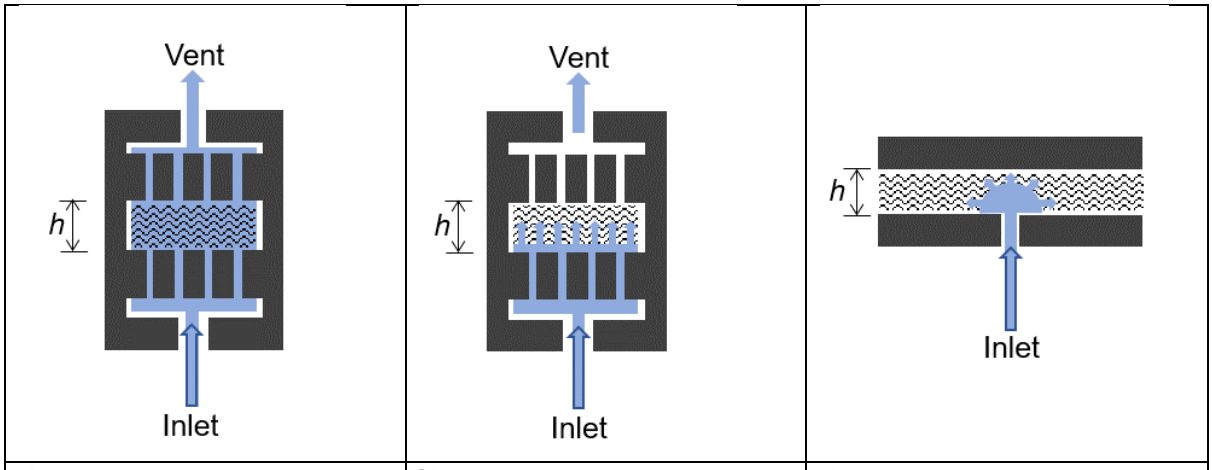

a) b) c)

Figure 1. Schematic diagrams of the principles of measurement in a) 1D saturated flow, b) 1D unsaturated flow, and c) 3D unsaturated flow.

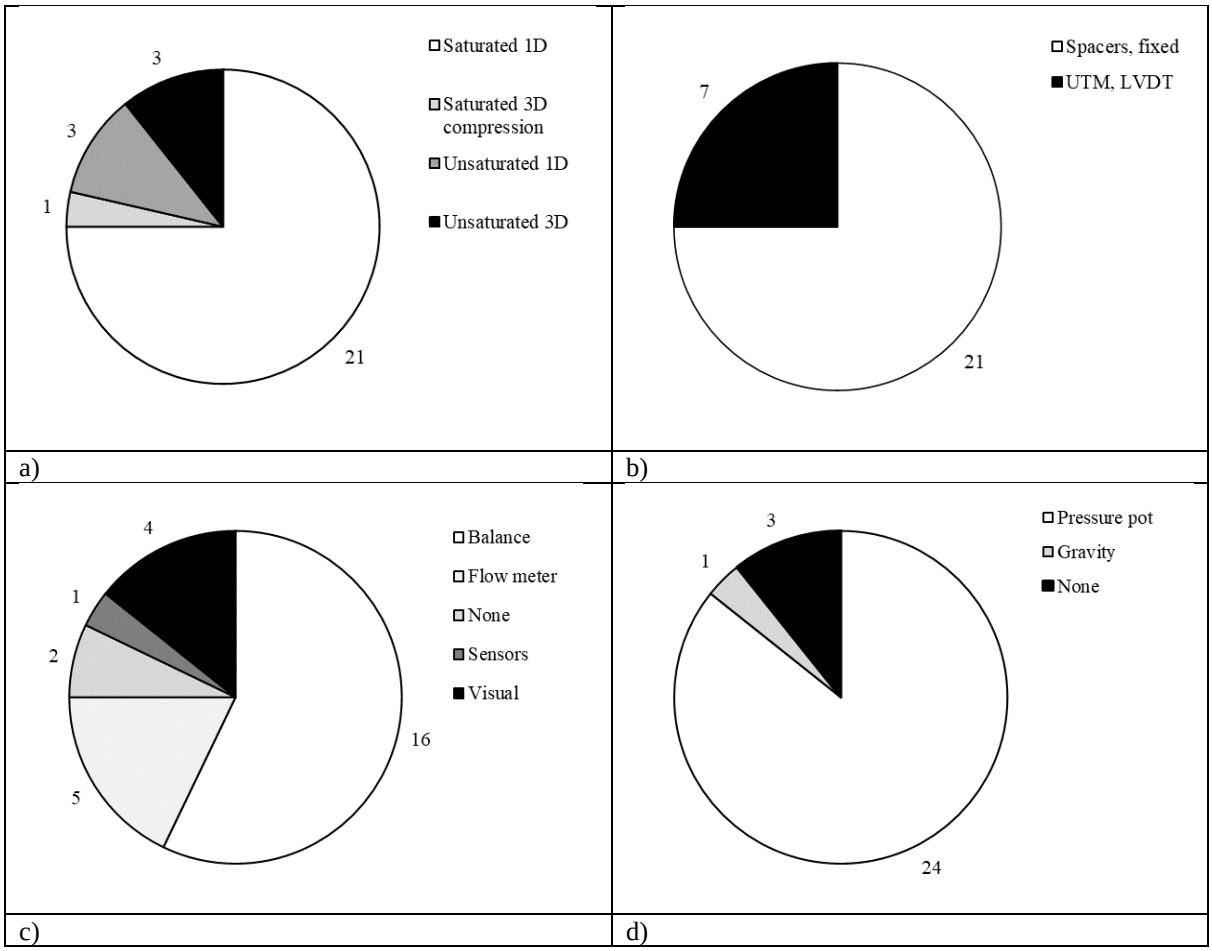

a) b) c) d)

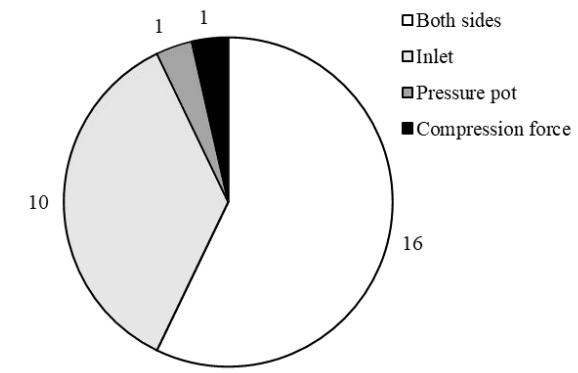

e)

Figure 2. Numbers of participants using different a) Specimen saturation and flow geometry, b) Thickness control, c) Flow rate measurement or flow front tracking, d) Pressure control and e) Pressure measurement location. The following abbreviations are used here: UTM (Universal Test Machine); LVDT (Linear Variable Differential Transformers).

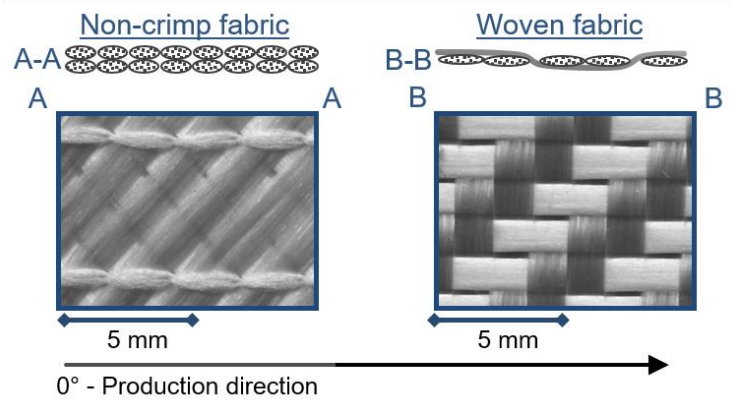

Figure 3. Images of the non-crimp fabric (left) and woven fabric (right) used in this benchmark study

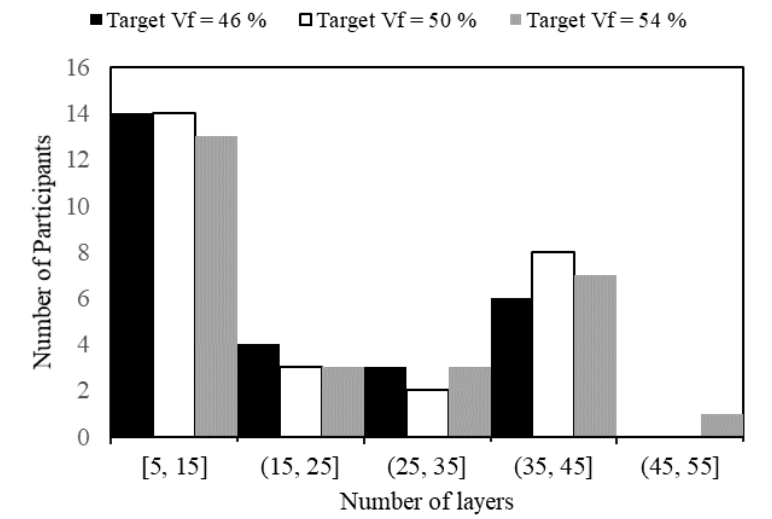

a)

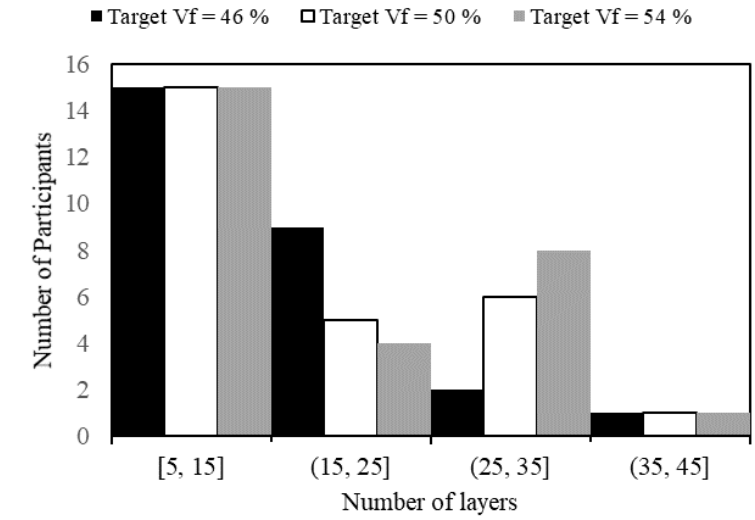

b)

Figure 4. Participant distribution for the number of layers used at different target fibre volume fractions for a) Woven fabric and b) NCF. Here, the following notation is used for intervals of numbers of layers, n; [n_1, n_2]: $n_1 \leq n \leq n_2$; (n_3, n_4]: $n_3 < n \leq n_4$.

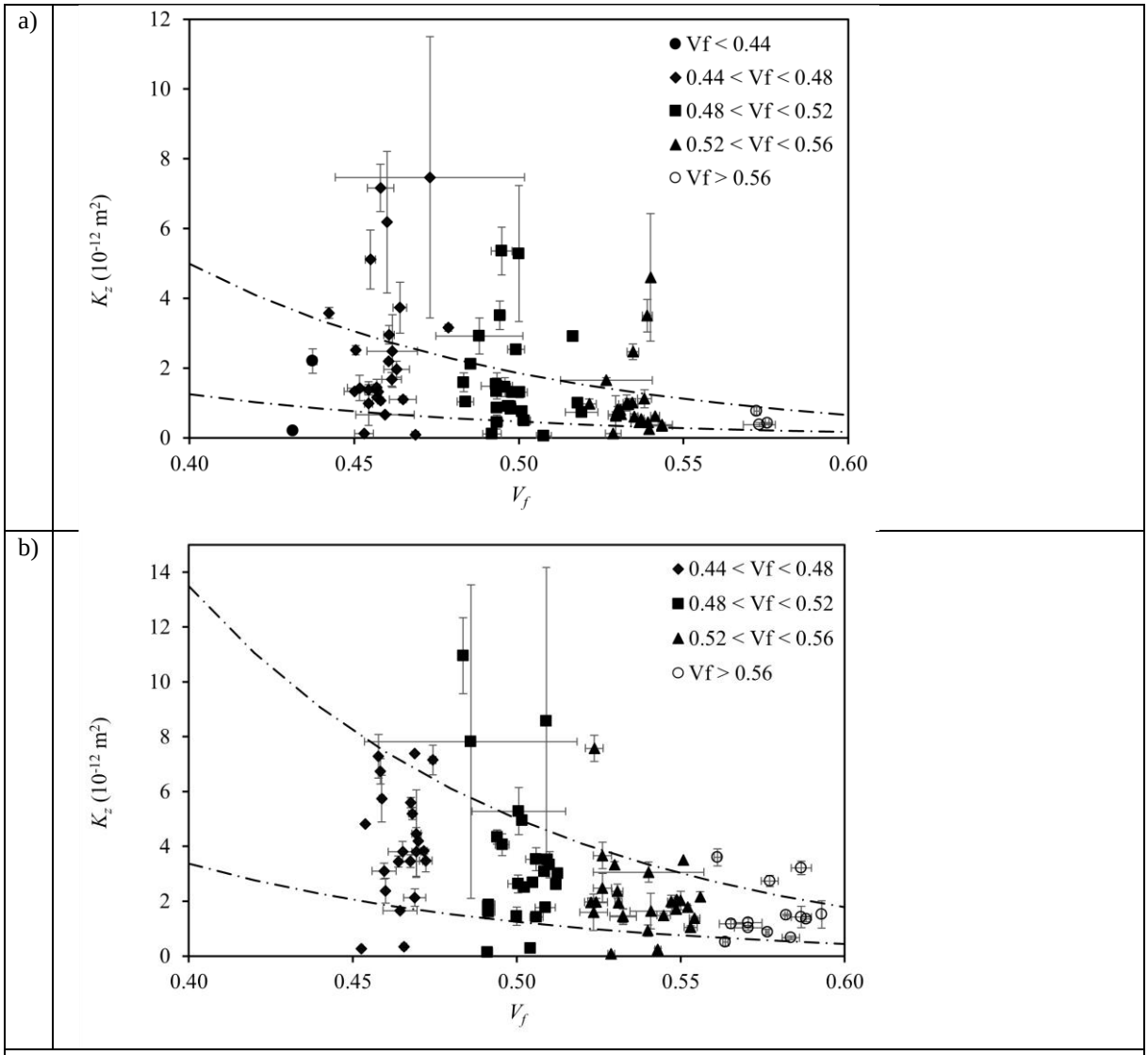

Figure 5. Out-of-plane permeability, K_z, as a function of the fibre volume fraction, V_f, for all participants. The target fibre volume fractions were 0.46, 0.50 and 0.54. a) Woven b) NCF. Average values and standard deviations are given. Dashed lines indicate a band of values where the ratio between upper and lower bound is 4.

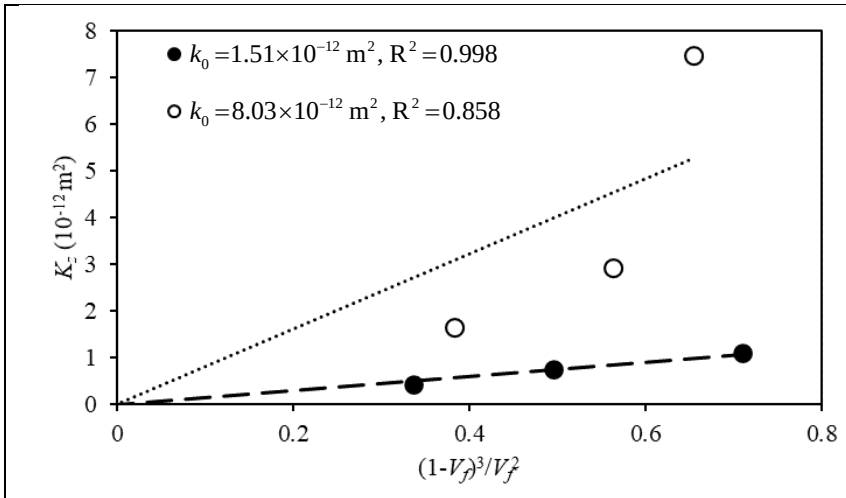

Figure 6. Two examples of Kozeny-Carman equation fit to measured permeability data: Through-thickness permeability, K_z, as a function of $(1-V_f)^3/V_f^2$. Both examples relate to the woven fabric (participants 1 and 2).

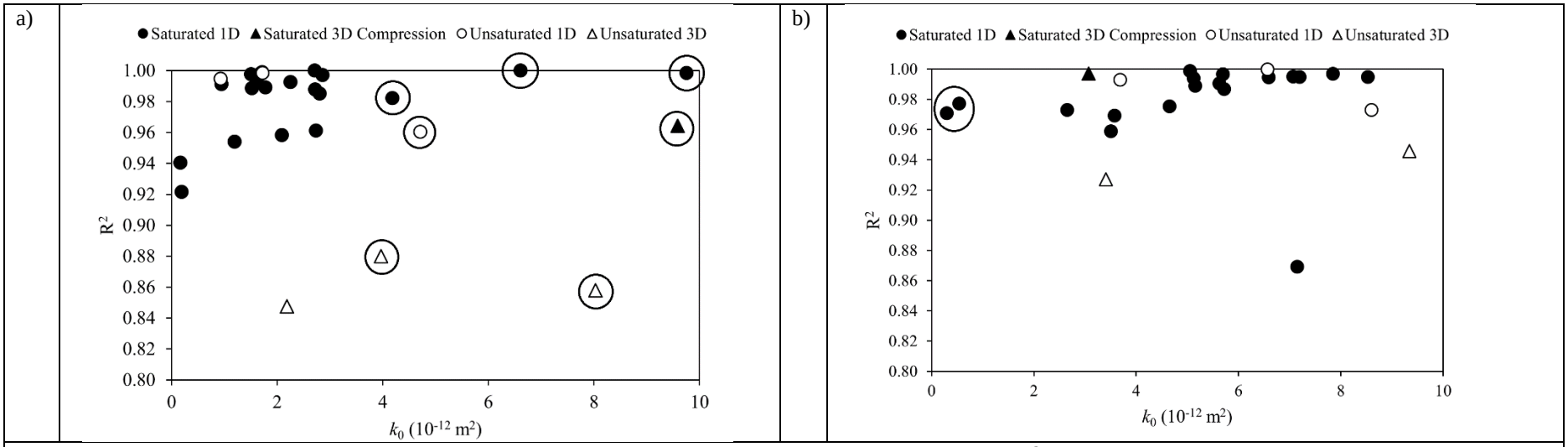

Figure 7. Kozeny-Carman equation factor, k_0, fitted to the participant permeability data with the corresponding R^2 for different experimental methods; a) Woven fabric and b) NCF. Values of k_0 identified as outliers are circled.

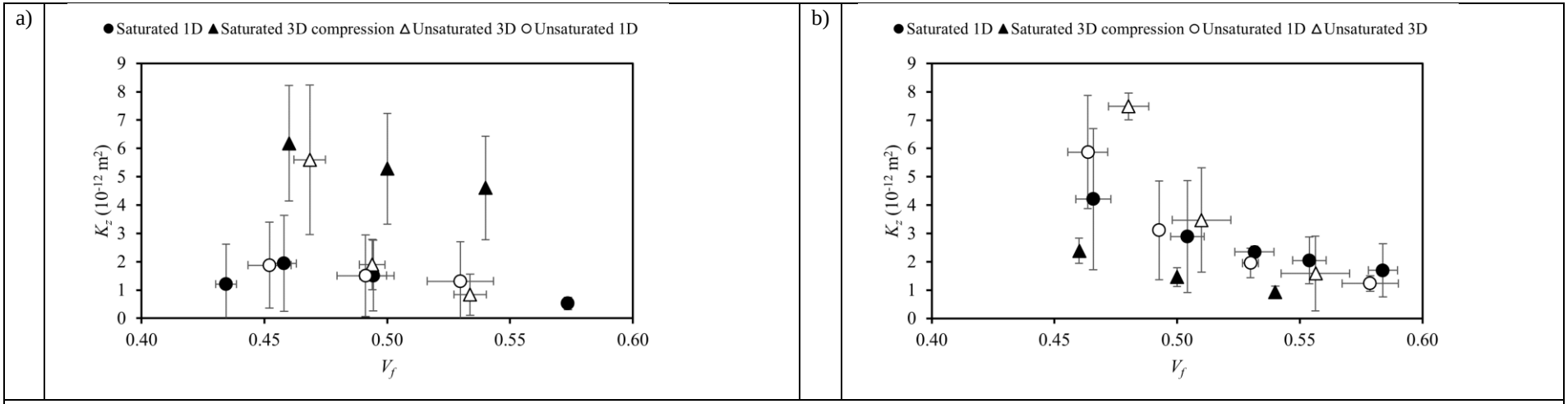

Figure 8. Through-thickness permeability, K_z, as a function of the fibre volume fraction, V_f. Comparison of different experimental methods; a) results for woven fabric; b) results for NCF.

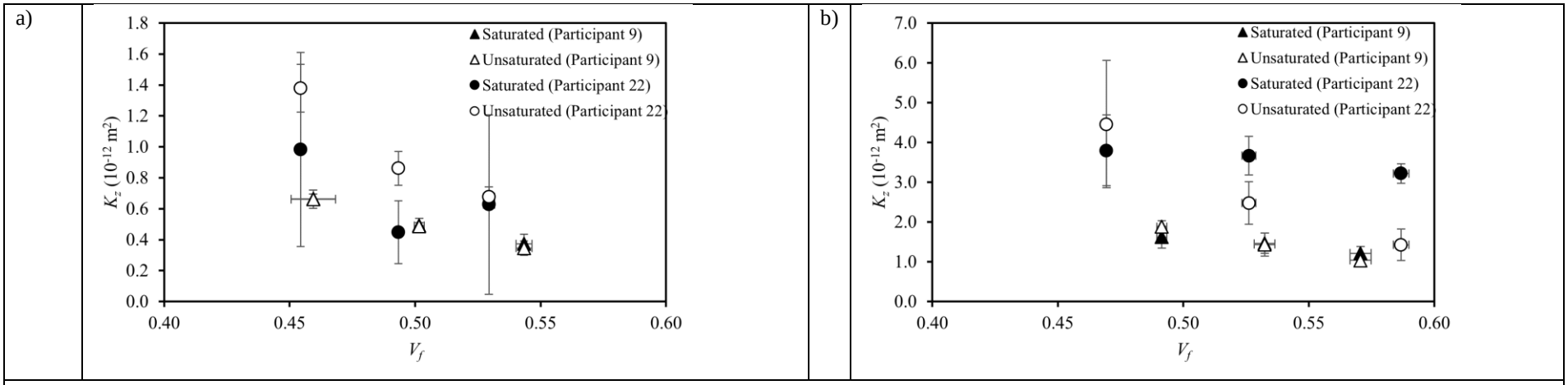

Figure 9. Through-thickness permeability, K_z, as a function of the fibre volume fraction, V_f. Comparison of different experimental methods for two participants (9 and 22); a) results for woven fabric; b) results for NCF.

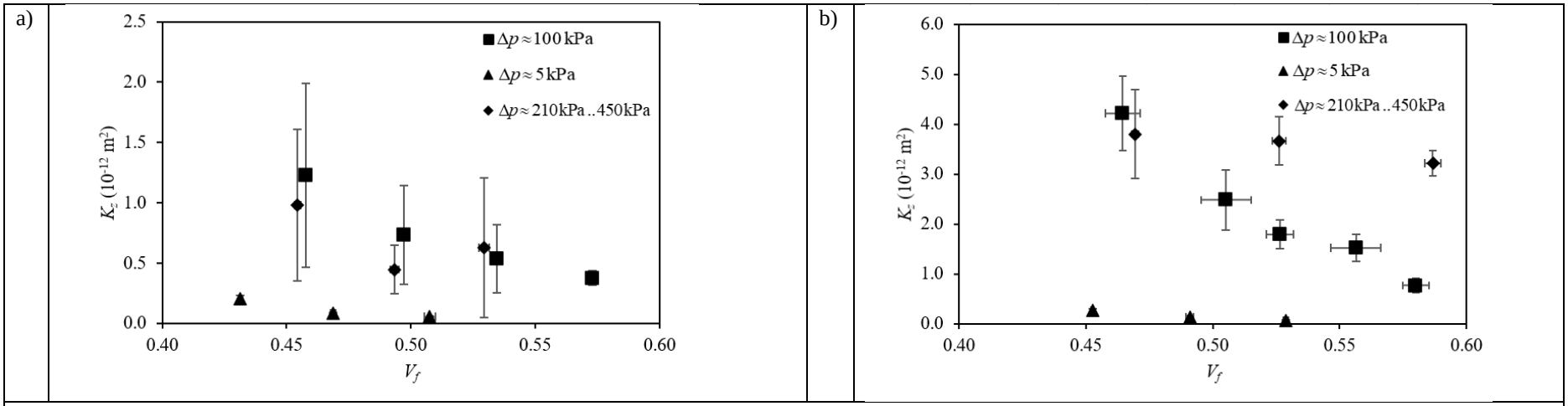

Figure 10. Through-thickness permeability, K_z, as a function of the fibre volume fraction, V_f. Comparison of values obtained at different pressure differences, Δp; a) results for woven fabric; b) results for NCF.

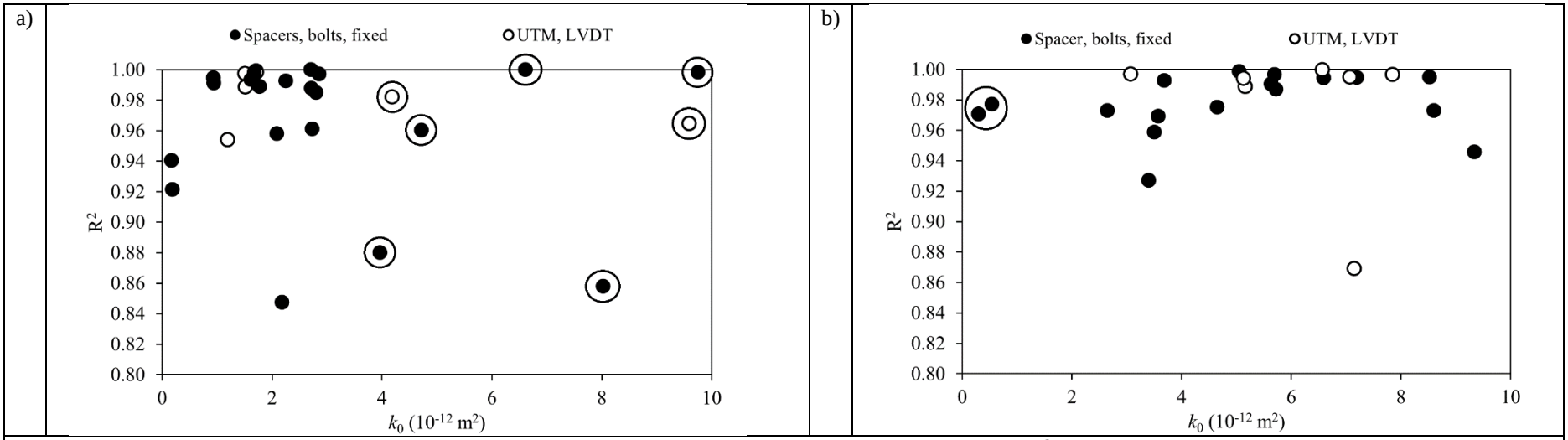

Figure 11. Kozeny-Carman equation factor, k_0, fitted to the participant permeability data with the corresponding R^2 for different methods of cavity height control; a) Woven fabric and b) NCF. Values of k_0 identified as outliers are circled. The following abbreviations are used here: UTM (Universal Test Machine); LVDT (Linear Variable Differential Transformers).

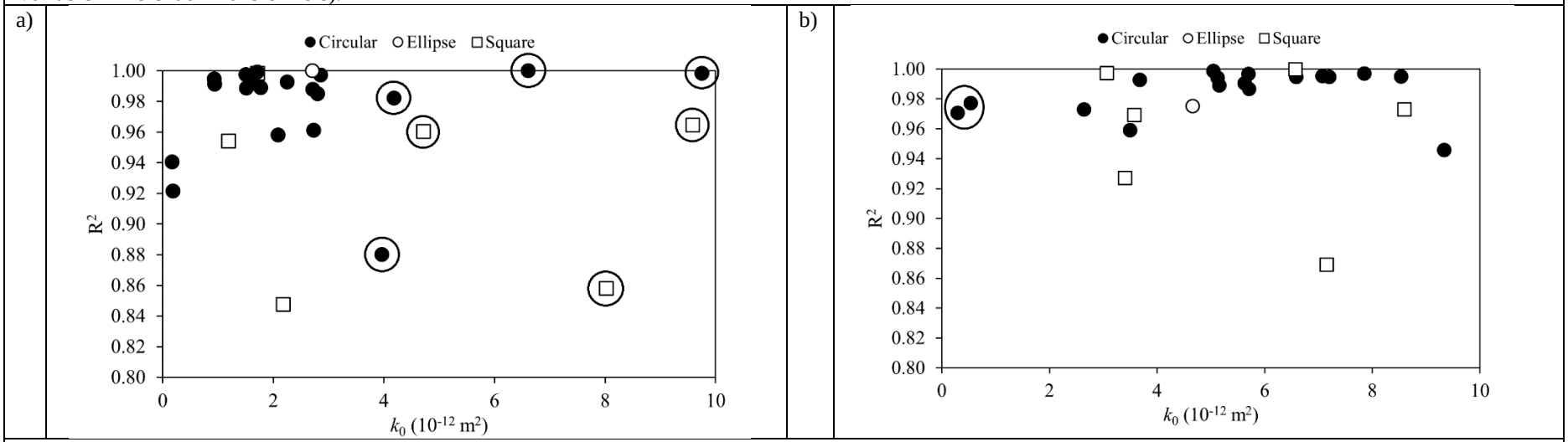

Figure 12. Kozeny-Carman equation factor, k_0, fitted to the participant permeability data with the corresponding R^2 for different specimen geometries; a) Woven fabric and b) NCF. Values of k_0 identified as outliers are circled.

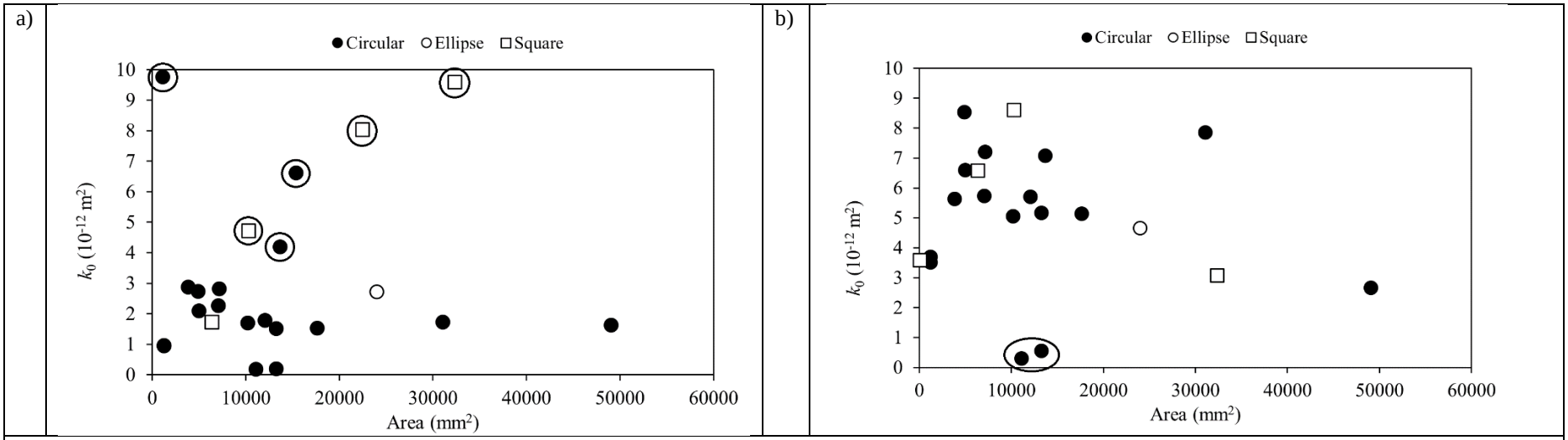

Figure 13. Kozeny-Carman equation factor, k_0, fitted to the participant permeability data as a function of the specimen area; a) Woven fabric and b) NCF. Values of k_0 identified as outliers are circled.

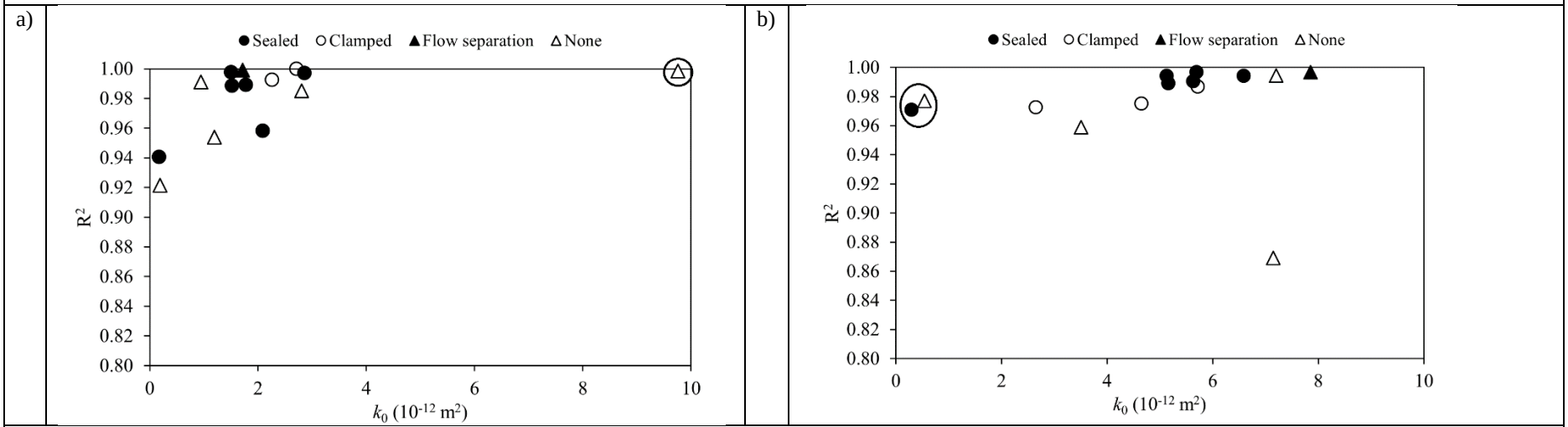

Figure 14. Kozeny-Carman equation factor, k_0, fitted to the participant permeability data with the corresponding R^2 for different methods of preventing race-tracking at the specimen edge; a) results for woven fabric; b) results for NCF. Values of k_0 identified as outliers are circled.

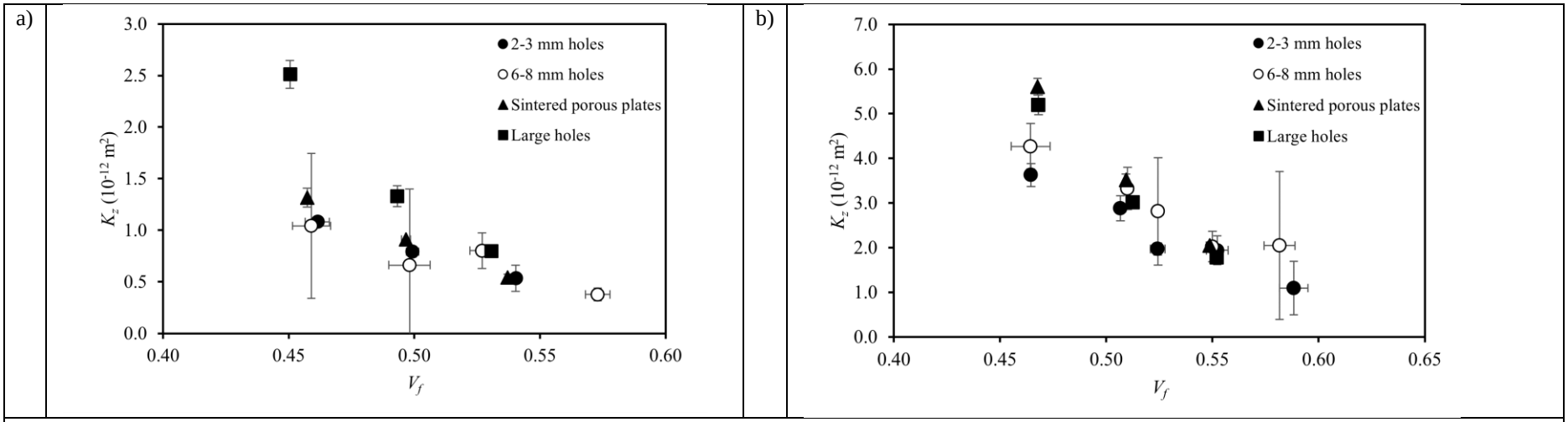

Figure 15. Through-thickness permeability, K_z, as a function of the fibre volume fraction, V_f. Comparison of values obtained using different compaction plates; a) results for woven fabric; b) results for NCF.

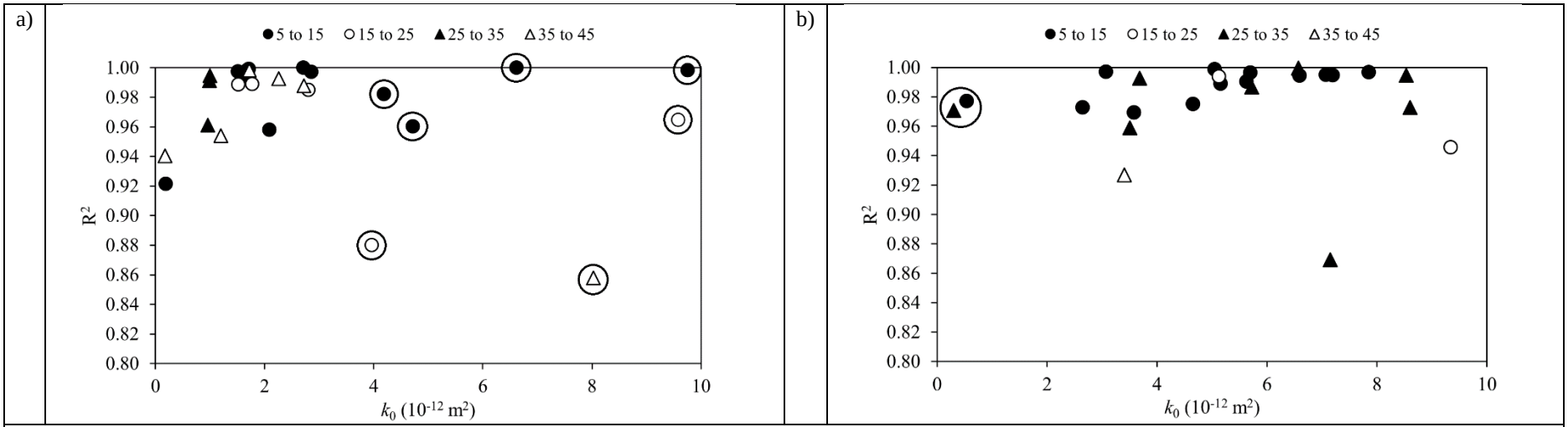

Figure 16. Kozeny-Carman equation factor, k_0, fitted to the participant permeability data with the corresponding R^2 for different numbers of fabric layers in specimens; a) Woven fabric and b) NCF. Values of k_0 identified as outliers are circled.

Table 1. List of participants.

Participant	Organisation	Department	Country
1	University of Auckland	Centre for Advanced Composite Materials	New Zealand
2	Brigham Young University	School of Technology	USA
3	TU Clausthal	Institute of Polymer Materials and Plastics Engineering	Germany
4	Université de Technologie de Compiègne	Roberval (Mechanics, Energy and Electricity) Laboratory	France
5	École Polytechnique Fédérale de Lausanne	Laboratory for Processing of Advanced Composites	Switzerland
6	FHNW University of Applied Sciences and Arts Northwestern Switzerland	Institute of Polymer Engineering	Switzerland
7	Fraunhofer IGCV	Composite Manufacturing Engineering	Germany
8	Institute de Soudure Composite Platform	Plateforme Composite	France
9	ITAINNOVA	Materials and Components Division	Spain
10	Institut für Verbundwerkstoffe GmbH	Manufacturing Science	Germany
11	Khalifa University of Science and Technology	Department of Aerospace Engineering	UAE
12	Koc University	Mechanical Engineering Department	Turkey
13	Montanuniversität Leoben	Department Polymer Engineering Science	Austria
14	McGill University	Structures and Composite Materials Laboratory	Canada
15	École Polytechnique Montréal	Department of Mechanical Engineering	Canada
16	TU München	Chair for Carbon Composites (LCC)	Germany
17	Centrale Nantes	Research Institute in Civil Engineering and Mechanics (GeM)	France
18	University of Nottingham	Composites Research Group, Faculty of Engineering	UK
19	National Physical Laboratory	Materials Testing Group	UK
20	Purdue University	Composites Manufacturing and Simulation Center	USA
21	Skolkovo Institute of Science and Technology	Centre for Design, Manufacturing and Materials	Russia
22	University Stuttgart	Institute of Aircraft Design	Germany
23	TENSYL		France
24	Universitat Politecnica de Valencia	Design for Manufacture Institute	Spain
25	Wuhan University of Technology	School of Materials Science and Engineering	China
26	ETH Zurich	Laboratory of Composite Materials and Adaptive Structures	Switzerland

Table 2. Details on test set-up for each participant.

Participant	Saturated or unsaturated flow	Flow geometry	Pressure control	Pressure measurement	Flow rate control	Flow rate measurement
1	saturated	1D	pressure pot	sensors on both sides of specimen	none	continuous decrease in mass of pressure pot at inlet
2	unsaturated	3D	pressure pot	sensor at pressure pot	none	visually determine time for fluid to reach opposite side of specimen and in-plane flow front propagation on injection side
3	saturated	1D	pressure pot	sensors on both sides of specimen	none	continuous increase in mass of resin pot at outlet
4	saturated	1D	pressure pot	sensors on both sides of specimen	none	continuous increase in mass of resin pot at outlet
5	saturated	1D	pressure pot	sensor at inlet of tool	none	continuous increase in mass of resin pot at outlet
6	saturated	1D	pressure pot	sensors on both sides of specimen	none	continuous increase in mass of resin pot at outlet
7	saturated	1D	pressure pot	sensors on both sides of specimen	none	continuous increase in mass of resin pot at outlet
8	saturated	1D	pressure pot	sensor at inlet of tool	none	continuous decrease in mass of pressure pot at inlet
9a	saturated	1D	pressure pot	sensor at inlet of tool	none	continuous increase in mass of resin pot at outlet
9b	unsaturated	1D	pressure pot	sensor at inlet of tool	none	sensors determine time for fluid to reach opposite side of specimen
10	saturated	1D	pressure pot	sensors on both sides of specimen	none	flow meter in feed line
11	saturated	1D	pressure pot	sensors on both sides of specimen	none	flow meter in feed line
12	saturated	1D	pressure pot	sensor at inlet of tool	none	continuous increase in mass of resin pot at outlet
13	unsaturated	3D	pressure pot	sensor at inlet of tool	none	flow meter in feed line and ultrasound detection of flow front
14	saturated	1D	pressure pot	sensors on both sides of specimen	none	continuous increase in mass of resin pot at outlet
15	saturated	1D	pressure pot	sensor at inlet of tool	none	continuous increase in mass of resin pot at outlet
16	saturated	1D	pressure pot	sensors on both sides of specimen	none	continuous increase in mass of resin pot at outlet
17	saturated	3D	none	compression force is recorded	specimen compaction	none
18	saturated	1D	none	sensors on both sides of specimen	gear pump	flow meter in feed line
19	saturated	1D	pressure pot	sensors on both sides of specimen	none	continuous increase in mass of resin pot at outlet
20	unsaturated	1D	pressure pot	sensor at inlet of tool	none	visually determine time for fluid to reach opposite side of specimen
21	unsaturated	3D	pressure pot	sensor at inlet of tool	none	visually determine time for fluid to reach opposite side of specimen and in-plane flow front propagation on injection side
22a	saturated	1D	pressure pot	sensors on both sides of specimen	none	flow meter in feed line
22b	unsaturated	1D	pressure pot	sensors on both sides of specimen	none	visually track flow front position
23	saturated	1D	pressure pot	sensors on both sides of specimen	none	continuous increase in mass of resin pot at outlet
24	saturated	1D	none	sensor at inlet of tool	unspecified pump	none
25	saturated	1D	pressure pot	sensors on both sides of specimen	none	continuous increase in mass of resin pot at outlet
26	saturated	1D	gravity driven	sensors on both sides of specimen	none	continuous increase in mass of resin pot at outlet

Table 3. Equations used in 3D unsaturated flow experiments and corresponding references, as given by participants.

Participant	Permeability calculation (unsaturated)	Reference
2	$K_z = \frac{\mu\varepsilon {b_z}^2}{6t\Delta p}\left[2\left(\frac{r_z}{b_z}\right)^3 - 3\left(\frac{r_z}{b_z}\right)^2 + 1\right]$, where $b_z = b_T\,[r_z\,(r_x\,r_y)^{-1/2}]$ b_T: characteristic dimension of spherical resin inlet r_x, r_y, r_z: dimensions of flow front in *x*-, *y*-, and *z*-directions	Mekic et al. [13]
13	$K_z = \left(\frac{z_f}{r_f}\right)^2 K_e$, where $r_f = \left(\frac{3m}{2\pi\rho\varepsilon}\right)^{\frac{1}{3}}$ and $z_f = z_k - z_k\frac{t-t_e}{t_s-t_e}$ $K_e = \frac{\mu\varepsilon r_0^2}{6\Delta pt}\left[2\left(\frac{r_f}{r_0}\right)^3 - 3\left(\frac{r_f}{r_0}\right)^2 + 1\right]$ z_f: flow front position in thickness direction r_f: flow front position in equivalent isotropic coordinates m: mass of injected fluid z_k: total specimen thickness t: measured time-of-flight t_e: time-of-flight for completely wetted material t_s: time-of-flight for dry material r_0: dimension of fluid inlet in equivalent isotropic coordinates	Becker et al. [14]
21	$F(\xi_f,\ \pi/2) = \frac{(K_xK_yK_z)^{1/3}\Delta pt}{r_0^2\mu\varepsilon}$ where $F(\xi_f, \pi/2) = F_1(\xi_f) + F_2(\xi_f)$ $F_1(\xi_f) = \frac{1}{6}\left\{(4\arctan e^{\xi_f} - \pi)\sinh^3\xi_f - \frac{1}{2}(\cosh 2\xi_f - 1) + 2\ln\cosh\xi_f\right\}$ $F_2(\xi_f) = \frac{1}{2}\{(4\arctan e^{\xi_f} - \pi)\sinh^3\xi_f - 2\ln\cosh\xi_f\}$ K_x, K_y: in-plane permeability values, measured in in-plane benchmark exercise [4] r_0: radius of circular injection gate ξ_f: curvilinear coordinate describing flow front	Mekic et al. [13]

Table 4. Details of tool design for each participant.

Participant	Material	Clamping mechanism	Fluid distribution	Cavity height adjustment	Cavity height range (mm)	Edge sealing
1	Aluminium	UTM	Perforated plates	Machine displacement	0-15	Yes
2	Acrylic	Bolts	None (Radial injection)	Spacers	Unlimited	N/A
3	Steel cylinder, Aluminium Honeycomb	Bolts	Honeycombs	Spacers	2-8	Yes
4	Steel	Bolts	Perforated plates	Spacers	1-30	No
5	PMMA casing, Aluminium cylinder, Aluminium Honeycomb	Bolts	Honeycombs	Spacers	0-30	No
6	PMMA casing, steel piston and lid, aluminium frame, aluminium honeycomb	Hydraulic Cylinders	Honeycombs	Spacers	5-40	Not stated
7	Steel and sinter metal	UTM	Sintered distribution structures	Machine displacement	0-7.5	None. Buffer zone separates edge flow.
8	Aluminium with steel spacers	Bolts & Compression with a Pneumatic Balloon	Perforated plates	Spacers	1-15	Edge compaction
9a	Aluminium	Bolts	Honeycombs	Fixed	8.3	No
9b	Aluminium	Bolts	Honeycombs	Fixed	8.3	N/A
10	Aluminium	Bolts	Perforated plates	Spacers	1-30	Edge compaction
11	Aluminium	UTM	Perforated plates	Machine displacement	0-10	Yes
12	Aluminium cylinder and plate, steel flanges	Bolts	Perforated plates	Spacers (fixed)	10.02-10.05*	Edge compaction
13	Steel	Pneumatic Cylinders	None (Radial Injection)	Spacers	8 (fixed)	N/A
14	Aluminium plate, Steel cylinder	Bolts	Perforated plates	Bolts	0-25.4	Not stated
15	Steel	Bolts	Perforated plates	Spacers	0-	No
16	Aluminium plates, steel assembly	Bolts	Perforated plates	Spacers	Unlimited	O-ring
17	Aluminium, PMMA	UTM	Perforated plate on one side	Machine displacement	1-30	No
18	Aluminium cylinder, Steel plates	Bolts	Perforated plates	Spacers	2-10	Yes
19	Aluminium, steel	UTM	Perforated plates	Machine displacement	0-30	TBC
20	PMMA	Bolts	No details	Spacers	3-30	N/A
21	PMMA	Bolts	None (Radial Injection)	Spacers	6 (fixed)	N/A
22a	Steel plates and acrylic	Bolts	Perforated plates	Machine displacement	9 (fixed)	No
22b	Steel plates and acrylic	Bolts	Perforated plates	Machine displacement	9 (fixed)	No
23	Technical Thermoplastics	Bolts	No details	Spacers	1-20	N/A
24	Aluminium	Bolts	No details	Bolts	0-30	Not stated
25	Steel	Bolts	No details	Spacers	1-70	Not stated
26	Steel	Bolts	Perforated plates	Spacers	9 (fixed)	Yes

Table 5. Specimen shape and dimensions used by different participants.

Participant	V_f	Shape	Dimensions (mm)	WF		NCF	
				h (mm)	n	h (mm)	n
1	$V_{f,1}$	Circular	130	2.91	12	2.91	8
	$V_{f,2}$			2.91	13	2.91	9
	$V_{f,3}$			2.91	14	2.91	10
2	$V_{f,1}$	Square	150	9	36	14.6	39
	$V_{f,2}$			9	39	14.6	42
	$V_{f,3}$			9	42	14.6	45
3	$V_{f,1}$	Circular	70	3.06	13	3.06	8
	$V_{f,2}$			3.06	14	3.06	9
	$V_{f,3}$			3.06	15	3.06	10
4	$V_{f,1}$	Circular	38	3	12	3	8
	$V_{f,2}$			3	13	3.5	10
	$V_{f,3}$			3	14	3.5	11
5	$V_{f,1}$	Circular	130	3	12	4.5	12
	$V_{f,2}$			3	13	4.5	13
	$V_{f,3}$			3	14	4.5	14
6	$V_{f,1}$	Circular	79	10	40	10	26
	$V_{f,2}$			10	43	10	28
	$V_{f,3}$			10	45	10	30
7	$V_{f,1}$	Circular	199	3.52	14	3.79	10
	$V_{f,2}$			3.24	14	3.48	10
	$V_{f,3}$			3.00	14	3.22	10
8	$V_{f,1}$	Circular	250	2.5	10	1.9	5
	$V_{f,2}$			2.3	10	1.75	5
	$V_{f,3}$			2.15	10	1.6	5
9	$V_{f,1}$	Circular	40	8.3	33	8.3	22
	$V_{f,2}$			8.3	36	8.3	24
	$V_{f,3}$			8.3	39	8.3	26
10	$V_{f,1}$	Ellipse	156x196	3.7	15	3.8	10
	$V_{f,2}$			3.5	15	3.8	11
	$V_{f,3}$			3.6	17	3.8	12
11	$V_{f,1}$	Circular	150	6.03	24	6.15	16
	$V_{f,2}$			5.55	24	5.65	16
	$V_{f,3}$			5.1	24	5.2	16
12	$V_{f,1}$	Circular	95	10	40	10	26
	$V_{f,2}$			10	45	10	30
	$V_{f,3}$			10	50	10	33
13	$V_{f,1}$	Square	170	--	--	--	--
	$V_{f,2}$			8.45	37	8.45	25
	$V_{f,3}$			8.45	40	8.45	27
14	$V_{f,1}$	Square	10	1.26	5	1.89	5
	$V_{f,2}$			1.16	5	1.74	5
	$V_{f,3}$			1.07	5	1.61	5
15	$V_{f,1}$	Circular	95.6	5.29	21	5.29	14
	$V_{f,2}$			5.29	23	4.48	13
	$V_{f,3}$			4.48	21	4.48	14
16	$V_{f,1}$	Circular	124	5.8	23	4.5	12
	$V_{f,2}$			5.8	25	4.5	13
	$V_{f,3}$			5.8	27	4.5	14
17	$V_{f,1}$	Square	180	2.51	10	3.78	10
	$V_{f,2}$			2.31	10	3.48	10
	$V_{f,3}$			2.14	10	3.22	10
18	$V_{f,1}$	Circular	80	3.05	12	3.05	8
	$V_{f,2}$			2.8	12	2.8	8
	$V_{f,3}$			2.6	12	2.6	8
19	$V_{f,1}$	Circular	132	3	12	3.5	10
	$V_{f,2}$			3	13	3.2	10
	$V_{f,3}$			3	14	3.0	10
20	$V_{f,1}$	Square	101.6	3	12	9.5	25
	$V_{f,2}$			3	13	9.5	27
	$V_{f,3}$			3	14	9.5	29
21	$V_{f,1}$	Circular	100	6	24	6	16
	$V_{f,2}$			6	26	6	17
	$V_{f,3}$			6	28	6	19
22	$V_{f,1}$	Square	80	9	36	9	24
	$V_{f,2}$			9	39	9	27
	$V_{f,3}$			9	42	9	30
23	$V_{f,1}$	Circular	100	7	27	7	18

	$V_{f,2}$			7	30	7	20
	$V_{f,3}$			7	33	7	22
24	$V_{f,1}$	Circular	140	3.02	12	3.03	8
	$V_{f,2}$			2.78	12	2.79	8
	$V_{f,3}$			2.57	12	2.58	8
25	$V_{f,1}$	Circular	114	3.01	12	3.01	8
	$V_{f,2}$			3.01	13	2.8	8
	$V_{f,3}$			3.01	14	3.2	10
26	$V_{f,1}$	Circular	119	9	36	9	24
	$V_{f,2}$			9	39	9	26
	$V_{f,3}$			9	42	9	28

Table 6. Kozeny-Carman equation fit analysis results. * indicates outliers identified using the Thompson Tau test.

Participant	Woven		NCF	
	k_0 (10^{-12} m^2)	R^2	k_0 (10^{-12} m^2)	R^2
1	1.51	0.998	5.16	0.989
2	8.03*	0.858*	11.82*	0.978
3	2.86	0.997	5.63	0.990
4	9.76*	0.998*	18.17*	0.988*
5	0.19	0.922	0.54*	0.977*
6	2.72	0.988	8.53	0.995
7	1.72	0.999	7.85	0.997
8	1.62	0.993	2.65	0.973
9a	0.95	0.991	3.51	0.959
9b	0.93	0.995	3.69	0.993
10	2.71	1.000	4.66	0.975
11	1.52	0.989	5.13	0.994
12	2.26	0.993	5.72	0.987
13	2.19	0.847	3.41	0.927
14	-	-	3.58	0.969
15	2.81	0.985	7.20	0.995
16	1.78	0.989	5.69	0.997
17	9.59*	0.964*	3.07	0.997
18	2.09	0.958	6.59	0.994
19	4.19*	0.982*	7.07	0.995
20	4.72*	0.960*	8.60	0.973
21	3.97*	0.880*	9.34	0.946
22a	1.19	0.954	7.15	0.869
22b	1.72	0.998	6.57	1.000
23	2.74	0.961	10.86*	0.837*
24	6.62*	1.000*	10.70*	0.998*
25	1.68	0.998	5.05	0.999
26	0.17	0.940	0.30*	0.971*